Relative impact of seasonal and oceanographic drivers on surface chlorophyll *a* along a Western Boundary Current

Jason D. Everett [a,b,c,*] Mark E. Baird [a,b] Moninya Roughan [b,d]

Iain M. Suthers [b,c] Martina A. Doblin [a,b]

[a] *Plant Functional Biology and Climate Change Cluster, Faculty of Science, University of Technology Sydney, PO Box 123 Broadway, Sydney NSW 2007, Australia*

[b] *Sydney Institute of Marine Science, Mosman NSW 2088, Australia*

[c] *Evolution & Ecology Research Centre, School of Biological Earth and Environmental Sciences, University of New South Wales, Sydney NSW 2052, Australia*

[d] *School of Mathematics and Statistics, University of NSW, Sydney NSW 2052, Australia*

Abstract

Strengthening Western Boundary Currents (WBCs) advect warm, low nutrient waters into temperate latitudes, displacing more productive waters. WBCs also influence phytoplankton distribution and growth through current-induced upwelling, mesoscale eddy intrusion and seasonal changes in strength and poleward penetration. Here we examine dynamics of chlorophyll *a* (Chl. *a*) in the western Pacific Ocean, a region strongly influenced by the East Australian Current (EAC). We interpreted a spatial and temporal analysis of satellite-derived surface Chl. *a*, using

a hydrodynamic model, a wind-reanalysis product and an altimetry-derived eddy-census. Our analysis revealed regions of persistently elevated surface Chl. *a* along the continental shelf and showed that different processes have a dominant effect in different locations. In the northern and central zones, upwelling events tend to regulate surface Chl. *a* patterns, with peaks in phytoplankton biomass corresponding to two known upwelling locations south of Cape Byron (28.5 °S) and Smoky Cape (31 °S). Within the central EAC separation zone, positive surface Chl. *a* anomalies occurred 65 % of the time when both wind-stress (τ_w) and bottom-stress (τ_B) were upwelling-favourable, and only 17 % of the time when both were downwelling-favourable. The interaction of wind and the EAC was a critical driver of surface Chl. *a* dynamics, with upwelling-favourable τ_W resulting in a 70 % increase in surface Chl. *a* at some locations, when compared to downwelling-favourable τ_W. In the southern zone, surface Chl. *a* was driven by a strong seasonal cycle, with phytoplankton biomass increasing up to 152 % annually each spring. The Stockton Bight region (32.25 to 33.25 °S) contained $\geq$20 % of the total shelf Chl. *a* on 27 % of occasions due to its location downstream of upwelling locations, wide shelf area and reduced surface velocities. This region is analogous to productive fisheries regions in the Aghulus Current (Natal Bight) and Kuroshio Current (Enshu-nada Sea). These patterns of phytoplankton biomass show contrasting temporal dynamics north and south of the central EAC separation zone with more episodic upwelling-driven Chl. *a* anomalies to the north, compared with regular annual spring bloom dynamics to the south. We expect changes in the strength of the EAC to have greater influence on shelf phytoplankton dynamics to the north of the separation zone.

Key words: Phytoplankton, Western Boundary Current, separation zone, upwelling, eddies, spring bloom, wind, retention

---

* Corresponding Author
Email address: Jason.Everett@uts.edu.au (Jason D. Everett).

1 Introduction

1.1 Phytoplankton, Boundary Currents and Fisheries

Western Boundary Currents (WBC) are among the most intensive transport features in the world's oceans (Loder et al., 1998) and strongly influence the circulation and water mass properties of the adjacent continental shelf and coastal ocean. WBCs advect warm, low nutrient waters poleward and are warming faster than the global ocean, resulting in their poleward intensification (Wu et al., 2012). WBCs are often thought of as unproductive relative to Eastern Boundary Currents, however they drive upwelling of nutrient rich water and generate eddies and thus support some of the most productive habitats in the world's oceans (Olson, 2001). These oceanographic processes can profoundly influence phytoplankton dynamics by altering the availability of light and nutrients and thereby generate considerable phytoplankton biomass and substantial fisheries (Ryther, 1969; Bakun et al., 1982; Logerwell and Smith, 2001).

Worldwide, 25 % of the primary productivity generated in upwelling systems directly sustains local fisheries (Pauly and Christensen, 1995). Small pelagic fish often dominate in upwelling ecosystems (Fréon and Cury, 2005), and their populations are crucial to the transfer of energy from phytoplankton to higher trophic levels (Cury, 2000). As there are few trophic linkages between small pelagic fish and the plankton community, upwelling events can quickly lead to increases in productivity. Understanding how and when changes in phytoplankton biomass occur is therefore important for understanding the critical habitat and stock fluctuations of these species.

1.2 East Australian Current

The East Australian Current (EAC) is the WBC of the South Pacific subtropical gyre and strongly influences the biogeochemical properties of southeast Australian continental shelf waters (Nilsson and Cresswell, 1981; Hassler et al., 2011). The EAC can encroach onto the shelf and displace continental shelf waters, drive upwelling of nutrient rich waters into the euphotic zone and generate eddies. EAC flow varies seasonally (Ridgway and Godfrey, 1997), but upwelling is generally persistent in the region south of Cape Byron (28.5 °S; Oke and Middleton, 2000) and Smoky Cape (31 °S; Roughan and Middleton, 2002) where the shelf narrows and the EAC exhibits its greatest speeds (Fig. 1). In these areas, upwelling is often visible as cooler surface water (Fig. 2). The EAC generally separates from the coast near 32 °S (Godfrey et al., 1980), with the majority of the flow retroflected eastward to form the Tasman Front, while the remaining flow continues southwards at a reduced velocity, as the EAC Extension (Hill et al., 2011). The separation zone creates a major north-south disjunct in the physical and biological properties of shelf water. To the north of the separation zone, oligotrophic EAC water mixes with upwelled water, while the south is dominated by Tasman Sea water (Baird et al., 2008).

The dynamic oceanography in this region has proved challenging for interpreting biological time series at a single location (Thompson et al., 2009). Unlike the regular seasonal cycles seen in some temperate Northern Hemisphere waters (Winder and Cloern, 2010), the phytoplankton spring bloom along the southeast Australian continental shelf is more irregular and appears to be related to the variability in the strength of the EAC (Hallegraeff and Jeffrey, 1993). Furthermore, phytoplankton blooms at small spatial scales of-

ten coincide with episodic slope water intrusions (Ajani et al., 2001) and EAC ecosystem models show increased growth and biomass within upwelling zones (Baird et al., 2006). Additionally EAC coastal eddies can drive nutrient rich slope water up onto the continental shelf (Tranter et al., 1986) and generate upwelling in their centre (Hassler et al., 2011; Everett et al., 2011), both of which can initiate plankton blooms. In eastern boundary currents such as the California Current, fluctuations in phytoplankton biomass are primarily driven by changes in wind-driven upwelling (Largier et al., 2006) and are strongly correlated to alongshore fish yield (Ware and Thomson, 2005). In WBCs, the link between oceanographic processes and Chl. *a* is more complex due to the combination of eddy activity and wind- and current-driven upwelling.

In light of this dynamic oceanographic context, we conducted an analysis of satellite-derived Chl. *a* using a hydrodynamic model, a wind-reanalysis product and an eddy-census in order to identify and partition the relative contribution of upwelling, eddies and seasonality to the observed patterns in Chl. *a*. Our aim was to: 1) quantify the spatial patterns of Chl. *a*, 2) examine the temporal effects of annual and seasonal cycles on Chl. *a* and 3) quantify the relative contribution of wind stress, bottom stress and eddy encroachment to Chl. *a* anomalies. Understanding the oceanographic processes driving phytoplankton biomass (surface Chl. *a*) is a first step to understanding the biological consequences of EAC variability.

2 Methods

The study domain was in the western Tasman Sea (Fig. 1) and extended from 27.75 °S to 37.75 °S, spanning subtropical and temperate latitudes, across the

continental shelf (0–200 m), continental slope (200–2000 m) and continental rise (2000–4000 m). This domain encompasses where the EAC is most cohesive in the north and includes a region of intense eddy activity (Everett et al., 2012). To examine spatial patterns in phytoplankton biomass, the domain was separated into twenty 0.5° latitudinal bands (Table 1), and the continental shelf (hereafter referred to as 'shelf'), continental slope (slope) and continental rise (rise) were analysed separately.

2.1 Satellite Chlorophyll a

Satellite remotely-sensed Chl. *a* (mg m^{-3}) was obtained from the Moderate Resolution Imaging Spectroradiometer Aqua Satellite (MODIS-Aqua; 2012.0 OC3 4 km L3) for the period 2003-2010. To maximise the temporal resolution, but minimise the data gaps, 8 day composite data was used. The pixels closest to the coast in an alongshore direction were removed from the analysis to exclude the effect of land or riverine inputs to the coastal zone. As a result, the minimum distance to the coast was 4 km, and sometimes further due to the masking of pixels which were partially obstructed by the land. The pixels which fell within each latitudinal band were spatially averaged using a geometric mean, to generate a Chl. *a* value for the shelf, slope and rise every 8 days. A long-term average Chl. *a* of all available data was calculated for each latitudinal band. The geometric mean, rather than the arithmetic mean, was used because the Chl. *a* concentration in shelf waters is generally log-normally distributed (Mouw and Yoder, 2005), which is also true of the dataset used in this study. In addition, the geometric mean has the advantage of reducing the effect of outliers on the mean.

Monthly and seasonal climatologies for each latitudinal band were also cal-

culated for the study period (8 years) by taking the geometric mean Chl. *a* for each calendar month or season respectively. Chl. *a* anomalies were calculated by subtracting the monthly climatology for each latitude from the temporal (8-day) value at that latitudinal band. The 0.5° latitudinal bands are referenced in the text by their central latitude (32 °S refers to 31.75-32.25 °S). The proportion of total shelf Chl. *a* (%) was calculated as the Chl. *a* at each latitude divided by the total shelf Chl. *a* within the domain for each time step. The average spring increase in Chl. *a* (%) was calculated as the percentage change at each latitude from the autumn (March-May) to spring (September-November) climatology.

To assess differences between latitudinal bands, the satellite-derived Chl. *a* was tested for autocorrelation using MATLAB R2013a. Successive autoregressive models were fitted by ordinary least squares, retaining the last coefficient of each regression. Autocorrelation was not present after 3 lags (24 days). Therefore every fourth data point was sub-sampled for a one-way Analysis of Variance of Chl. *a* amongst latitudinal bands. Differences were compared using Tukey's honestly significant difference criterion.

The dominant modes of variability of Chl. *a* and how those modes varied with time were examined using a wavelet analysis (Torrence and Compo, 1998). A wavelet analysis decomposes a time-series into time/frequency space simultaneously, highlighting periodic signals within the series and how these signals vary with time. A Morlet Wavelet was used and global power spectra were calculated using the MATLAB toolbox developed by Torrence and Compo (http://atoc.colorado.edu/research/wavelets/). The 95 % confidence intervals were calculated from a χ^2 test using the red-noise background spectrum.

2.2 Bottom and Wind Stress

Bottom stress (τ_b) and wind stress (τ_w) are measures of the force acting on the bottom and surface of the ocean respectively. When acting in an alongshore direction, these shear stresses act to move water towards or away from the coast, in turn driving downwelling or upwelling respectively. The EAC is considered to be an upwelling favourable current, flowing poleward on the western margin of an ocean basin in the Southern Hemisphere (see Fig. 1 in Roughan and Middleton (2004)). In this paper we discuss stresses as being neutral, upwelling- or downwelling-favourable. The τ_b calculated in the BRAN simulations is a result of the interaction of all physical processes (EAC mean flow, mesoscale eddies and wind), while τ_W was derived only from surface wind velocities.

The τ_b were calculated from bottom velocities which were derived from the Bluelink ReANalysis (BRAN) system (Version 2.2). BRAN has a resolution of 0.1° and involves the integration of a global ocean model that is eddy-resolving around Australia and includes sequential assimilation of altimetry, SST and Argo temperature and salinity observations (Oke et al., 2005, 2008; Schiller et al., 2008). An analysis of the variability in BRAN was completed (Oke et al., 2012, 2013) and was slightly higher than the observed variability at locations away from the core of the EAC. A comparison of modelled and observed volume transports of the EAC region however showed good agreement (within one standard deviation) for both mean and maximum transports (Oke et al., 2012). The analysis indicates that the estimates of EAC velocities which are used within this study are likely to be reasonable and reflect the observed velocities within our study region.

Bottom velocities from the centre of each latitudinal band at the edge of the continental shelf (∼200 m depth) are used for the period January 2003 to May 2008 (end of BRAN 2.2 simulation). The bottom velocities were temporally averaged over the first 4 days of the 8-day Chl. *a* time-step. The τ_B (N m^{-2}) at a given bottom velocity (V_B) is:

$$\tau_B = C_d V_B |V_B| \rho \tag{1}$$

where C_d is the drag co-efficient (2.5×10^{-3}), V_B is the north-south bottom velocity at the shelf edge rotated to the alongshore direction (m s^{-1}) and ρ is density of seawater (1025 kg m^{-3}). In addition, the surface velocity for the domain was extracted from BRAN and an average surface velocity calculated for January 2003 to May 2008 (Fig. 1B).

The τ_W were extracted from the European Centre for Medium-Range Weather Forecasts (ECMWF) wind re-analysis atlas (ERA-40) (Uppala et al., 2005) at the same locations as τ_B (above). As for τ_B, the wind stresses were temporally averaged over the first 4 days of the 8-day Chl. *a* time-step.

Upwelling- and downwelling-favourable stresses were defined differently.For τ_W, $\tau \leq$ -0.04 N m^{-2} was considered upwelling-favourable and $\tau \geq$ 0.04 N m^{-2} was considered downwelling-favourable (Wood et al., 2012). Values of -0.04 $\leq \tau \leq$ 0.04 N m^{-2} were considered neutral. For τ_B, $\tau \leq$ -0.08 N m^{-2} was considered upwelling-favourable and $\tau \geq$ 0.08 N m^{-2} was considered downwelling-favourable. A τ_B of 0.08 corresponds to V_B of 0.18 m s^{-1}. Using 2 years of ADCP mooring data, Schaeffer et al. (2013) showed that the mean V_B is -0.1 m s^{-1} with maximums of -0.4 m s^{-1} during periods of strong southward current intrusions. Hence we are confident that this bottom velocity

is reasonable on the shelf, upstream of the EAC separation.

To assess the relative importance of different oceanographic processes, the time-series of Chl. *a* biomass and anomalies in each latitudinal band was compared to the corresponding τ_B and τ_W at the same location with no spatial lag. We repeated the analysis, by lagging Chl. *a* by 1-2 latitudinal bands at each time-step to account for the southward movement of phytoplankton due to EAC flow, but this did not improve our ability to explain the Chl. *a* variability, so simultaneous upwelling and Chl. *a* locations are reported. The number of situations which had each combination of upwelling/downwelling τ_B and τ_W was also calculated.

2.3 Eddy Distribution

The third process influencing phytoplankton in the region was eddies. When eddies encroach onto the shelf, they tend to divert the flow of the EAC onshore (anticyclonic eddies) or further offshore (cyclonic eddies). When a cyclonic eddy encroaches onto the shelf, it drives a τ_B which is downwelling-favourable on the coastal (western) side. When an anticyclonic eddy encroaches onto the shelf, it drives an upwelling-favourable τ_B on the coastal (western) side.

In order to use observations where possible, eddy properties (location of eddy centre and radius) were extracted from a global census of Sea Surface Height (SSH) fields derived from altimetry (Chelton et al., 2011; Everett et al., 2012). Due to the filtering of SSH fields, the eddy dataset contains only mesoscale eddies (>80 km diameter). For a full discussion of the methods used to identify and track eddies see Chelton et al. (2011). The proximity of eddies to each latitudinal band was calculated from the eddy edge, as determined by the

eddy-centre and radius.

In this study we have used both observations (Satellite-derived Chl. *a* and eddies), and models where observations were not available (τ_B and τ_W). It should be noted that each of the datasets used in this analysis were produced at different spatial and temporal resolutions. As a result, the satellite-derived Chl. *a* and eddy data were analysed for the period 2003-2010. Bottom-stress and wind-stress were however, only available up to May 2008. As a result, when analysing Chl. *a* with respect to bottom- and wind-stress only 2003-2008 was included.

3 Results

3.1 Spatial Patterns of Chlorophyll a

There was a strong latitudinal gradient in Chl. *a* along the length of the study domain. The highest average Chl. *a* for each latitudinal band across all years (0.55 mg m^{-3}) occurred at the most southerly latitude (37.5 °S; Fig. 3A; Table 2). Chl. *a* was highest on the shelf, declining by 25-60 % across the slope and by a further 6-17 % across the rise. Chl. *a* on the slope and rise increased 181 and 166 % respectively from north to south (Fig. 3B,C).

On the shelf, Chl. *a* was elevated at 3 distinct locations, centred at 29/29.5 °S, 32 °S and 37.5 °S (Fig. 3A), with mean (± SD) Chl. *a* of 0.38/0.38 (2.81/2.61), 0.44 (2.70) and 0.55 (2.12) mg m^{-3} respectively ($F_{19,1787}$=9.86, P<0.001). Each of these three regions are bounded to the north by regions of significantly lower Chl. *a* (28.5 °S, 31 °S and 34 °S) where mean (± SD) Chl. *a* was 0.26 (2.30), 0.30 (2.25) and 0.31 (1.92) mg m^{-3} respectively. The standard deviation

(Table 2) indicates higher variability at the locations of elevated Chl. *a* in the north (29 and 32 °S). To the south, the greatest variability (2.49) occurred at 35.5 °S. As a result of these observations, the shelf was separated into three zones for the remainder of the analysis: northern zone (28-30.5 °S), central zone (31-33.5 °S) and southern zone (34-37.5 °S).

3.2 Temporal Patterns of Chlorophyll a

While there was significant temporal variability in the Chl. *a* on the shelf throughout the year (Fig. 4A), latitudes with a higher mean biomass tended to show persistently elevated conditions through time regardless of season. For example, a high mean Chl. *a* (>1 mg m^{-3}) occurred frequently at 29 °S, 32 °S and 35.5-37 °S. There was little inter-annual variability in the mean Chl. *a* apart from in 2009 (Fig. 5A). In this year, Chl. *a* was 18-84 % greater in the northern and central zones compared to the average of all other years (2003-2008, 2010).

There was a rise in Chl. *a* during spring at most latitudes, with relatively low Chl. *a* in summer and autumn and intermediate Chl. *a* in winter (Fig. 5B). The mean spring bloom Chl. *a* increase (Table. 2) for the entire shelf was 76 %, however this was highly dependent upon latitude. At the southern, temperate end of the domain, Bermagui (∼36.5 °S) experienced a spring bloom increase of 152 %, while in the northern subtropical zone, Urunga (∼30.5 °S), experienced a spring increase of only 27 % during 2003-2010. On average, the spring bloom in the northern zone resulted in a Chl. *a* increase of 27-65 %, in the central zone there was an increase of 28-107 %, while in the southern zone the spring bloom resulted in a 52-152 % Chl. *a* increase.

The dominant frequency of variability in Chl. *a* at sites within the the northern (29°S) and central zones (32°S) was short periods of less than 30 days, which occurred many times a year throughout the time series (Fig. 6A/B). These were significant at the 95 % confidence limit (χ^2 test) as indicated by the black contours in Fig. 6A/B and the Global Power Spectrum (Fig. 6D/E) which indicates the time-averaged intensity at each period. In the southern zone (36°S) there was a significant annual cycle corresponding to the spring bloom (Fig. 6C) that is also visible as a large peak in the Global Power Spectrum at 365 days (Fig. 6F).

3.3 Oceanographic Drivers of Chlorophyll a dynamics

In addition to the seasonal variability, oceanographic processes had a large role in determining the patterns in surface Chl. *a*. Upwelling-favourable bottom-stress (τ_B) and wind-stress (τ_W) resulted in increased Chl. *a* at most locations north of the separation zone, when compared to downwelling-favourable τ_B and τ_W (Fig. 5C). In the northern and central zones, mean Chl. *a* increased 3-53 % and 5-39% respectively when τ_B was upwelling-favourable (Fig. 5C). Only Urunga and Smoky Cape (30.5 and 31 °S) had a decreased mean Chl. *a* (-5 and -11 %) during upwelling-favourable τ_B. In the southern zone, upwelling-favourable bottom-stress (τ_B) had a weaker effect where Chl. *a* changed between -39 % and + 43 % (Fig. 5C).

Winds had strong role in the surface expression of Chl. *a*. Along the coast, winds were predominately downwelling-favourable (Table 1) which often suppressed surface Chl. *a*. In contrast when winds were upwelling-favourable, they often resulted in an increase in Chl. *a*. This was particularly apparent at Evans Head (29 °S) and Diamond Head (32 °S), where upwelling-favourable τ_W re-

sulted in an increase in Chl. *a* of 43 % and 69 % respectively when compared to Chl. *a* during downwelling-favourable τ_W (Fig. 5C). In the northern and central zones, Chl. *a* increased 13-54 % and 8-68 % when τ_W was upwelling-favourable (Fig. 5C).

Within the central zone, the presence of upwelling-favourable anticyclonic eddies resulted in 3-49 % higher Chl. *a* than the presence of downwelling-favourable cyclonic eddies between 31.5 and 33.5 °S (Fig. 5D). Only 31 °S showed a decline (3 %) during the presence of upwelling-favourable anticyclonic eddies. The largest difference in Chl. *a* between the presence of cyclonic and anticyclonic eddies occurred in the north at 29 °S where there was an increase of 77 %. In the southern zone, the presence of cyclonic eddies resulted in a 3-22% increase in Chl. *a* (Fig. 5D).

Examining the simultaneous occurrence of different upwelling/downwelling processes revealed the most favourable conditions leading to positive Chl. *a* anomalies, and those which led to negative Chl. *a* anomalies. Within the central zone, where upwelling favourable conditions resulted in the largest change in Chl. *a* (32-33.5 °S; Fig. 5), upwelling-favourable τ_B and τ_W resulted in a positive Chl. *a* anomaly 65% of the time (Table 3). When τ_B was upwelling-favourable but τ_W was downwelling-favourable, positive Chl. *a* anomalies only occurred on 38 % of occasions. Interestingly, an upwelling wind and downwelling current resulted in a positive Chl. *a* anomaly 58 % of the time, however this situation only occurred on 12 of 970 occasions within this region. A downwelling wind and current had the lowest proportion of positive Chl. *a* anomalies (24 %).

To more closely examine the relative importance of different oceanographic processes, we conducted a case study at the separation zone (32 °S). This

region displayed upwelling-favourable winds on 0-10 % of occasions during the April-August period (Fig. 7A), compared with 20-45 % of the time from September-December. The presence of anticyclonic eddies in close proximity to the coast peaked in October (Fig. 7B), occurring on 25 % of occasions, along with an increase in Chl. *a* (Fig. 7C). Conversely, cyclonic eddies acted to dampen upwelling-favourable conditions by reducing or reversing upwelling-favourable τ_B (Fig. 7D). Upwelling-favourable τ_B in the presence of a cyclonic eddy was only observed on only 1 occasion during the study period (Fig. 7D), with the number of cyclonic eddies peaking in July when the occurrence of upwelling-favourable conditions was at its lowest (Fig. 7A).

Several different situations which led to positive and negative Chl. *a* anomalies within the separation zone (32 °S) were examined (Fig. 8A). Positive Chl. *a* anomalies persisted through February and March 2003 when both τ_W and τ_B were upwelling-favourable (Fig. 8B). In contrast, when τ_B was strongly upwelling-favourable in May-July 2004, there was a negative Chl. *a* anomaly due to downwelling-favourable τ_W (Fig. 8C). A similar situation occurred in mid-2005 (Fig. 8D), when τ_B was upwelling-favourable for the majority of the period (April-June) however it was only when τ_W became neutral or upwelling-favourable that there was a positive surface Chl. *a* anomaly. Additionally, a shift from upwelling-favourable to downwelling-favourable τ_B was often apparent when a cyclonic eddy encroached within 50 km of the shelf-edge such as in April 2003, February 2004 and July 2005 (Fig. 8A; blue squares).

4 Discussion

Distinct and persistent coastal habitats, as defined by surface Chl. *a* dynamics, occur along the southeast Australian continental shelf. The underlying processes driving these spatial and temporal patterns differ in the northern, central and southern zones. To the south, Chl. *a* is greater and there is strong seasonal variability dominated by a large spring bloom. In the northern and central zones, Chl. *a* is generally lower and more variable with episodic upwelling events and eddy intrusions driving changes in phytoplankton biomass. In particular, the central zone, which is dominated by the EAC separation acts as a border between the northern and southern ecosystems. These observations are consistent with the EAC separation affecting the connectivity and dispersal of coastal organisms (Roughan et al., 2011), the genetic structure of sea-urchin populations (Banks et al., 2007), microbial community composition (Seymour et al., 2012), the size-structure of zooplankton communities (Baird et al., 2008), the distribution of fisheries such as southern bluefin tuna (Hobday and Hartmann, 2006) and the diet of top predator species, particularly albacore and yellowfin tuna (Revill et al., 2009).

4.1 Temporal drivers of surface Chl. a

The southern zone had lower surface velocities and a reduced number of occasions with upwelling-favourable τ_W and τ_B compared to northern and central zones. As a result, the dominant processes driving Chl. *a* in the south were shown to be seasonal. Phytoplankton growth in the Tasman Sea is generally nitrogen-limited (Hassler et al., 2011) with the spring bloom to the south corresponding to a seasonal increase in dissolved nitrate and silicate in June-

September (Fig. 9A), a shallowing of the mixed-layer depth and the onset of warming sea-surface temperatures (Fig. 9B). This seasonal increase in nutrients is generally lower in the subtropical waters of the central and northern zones (Fig. 9A), and as a result the corresponding size of the spring bloom is not as large (Fig. 5). Furthermore, lower stocks of nutrients suggest the blooms in the central and northern zones were likely to be triggered by the delivery of nitrate and silicate into surface waters. The nutrient climatology suggests that nitrate is limiting as silicate accumulates in the surface waters during spring, while the nitrate is drawn down (Fig. 9A). The larger winter bloom in the northern zone, suggests that temperature may also be a limiting factor for phytoplankton growth, with the largest bloom in the south and central zone, where warming occurs later, not occurring until spring.

There was little inter-annual variability in mean Chl. *a* in the northern and central regions except for 2009. Throughout 2009, Chl. *a* was elevated along the length of the continental shelf for much of the year (Fig. 4). One possible explanation is the El Niño-Southern Oscillation (ENSO) which went through a rapid transition from La Niña to El Niño in 2009 with the SOI index decreasing from 17.1 to -14.5 between in November 2008 and February 2010 (Bureau of Meteorology, 2012). This transition was unusual because it marked a progression from the strongest warming signal (El Niño) yet recorded in the Pacific to a strong La Niña (Kim et al., 2011).

4.2 Upwelling and eddy encroachment

In the north and central regions, wind- and current-driven upwelling events shape Chl. *a* patterns. The physical mechanisms of the upwelling south of Cape Byron (28.5 °S) and Smoky Cape (31 °S) are well known and under-

stood (Tranter et al., 1986; Oke and Middleton, 2000; Roughan and Middleton, 2002). ADCP measurements within the domain estimated that upwelling-favourable conditions would be strongest north of the separation zone (Schaeffer et al., 2013), in good agreement with the modelled τ_B used in this study (Table 1). In addition, the known regions of strong upwelling (Cape Byron and Smoky Cape) had a high proportion of upwelling-favourable conditions (60 and 43% respectively).

Our analysis revealed that the simultaneous occurrence of upwelling-favourable τ_B and τ_W is a more efficient mechanism for increased Chl a than an individual upwelling process (Schaeffer et al., 2013; Tranter et al., 1986; Roughan and Middleton, 2004). Under this scenario, shelf waters are preconditioned by upwelling-favourable τ_B, enabling τ_W to more efficiently lift nutrients into the euphotic zone (Gibbs et al., 1998). Our analysis showed that concurrent upwelling-favourable τ_B and τ_W in the central zone resulted in a positive Chl. a anomaly on 68% of occasions. In agreement with previous studies (Schaeffer et al., 2013; Gibbs et al., 1998), these results highlight the importance of both the current and wind in generating upwelling along the southeast Australian coast.

The effect of eddy encroachment on the τ_B of the continental shelf edge are apparent with anticyclonic eddies often strengthening the upwelling conditions, and cyclonic eddies weakening or reversing the upwelling effect of the EAC flow. Tranter et al. (1986) identified the importance of eddies, particularly anticyclonic eddies, interacting with the shelf and driving slope waters into the surface layers. This 'eddy effect' was dependent on eddy-proximity to the coast and the direction of wind, with few eddy-generated slope-water intrusions between April and August when the winds are predominantly westward.

Rossi et al. (submitted) showed clear seasonality in wind-driven upwelling along this coast, with October-November exhibiting the highest number of days with an upwelling-favourable wind and May-June the lowest. Similarly, we found infrequent upwelling-favourable τ_W during the April-August period at the separation zone, compared with greater frequency from September-December. Due to the spatial resolution of the eddy census used in this study (Chelton et al., 2011), we are unable to comment on the impact of eddies, with a diameter of <80 km, on Chl. *a* along the shelf. These smaller eddies may be able to explain more of the Chl. *a* variability within this study, and have previously been shown to contain high Chl. *a*, zooplankton and larval fish (Everett et al., 2011; Mullaney and Suthers, 2013).

4.3 Implications of Chl. a for secondary production

Enrichment, retention and concentration mechanisms are vital for the survival of larval fish (Bakun, 1996), yet areas of retention and concentration are not always readily apparent in vigorous WBC systems such as the EAC. As a result, relationships between surface oceanography and fish catches generally have relatively low explanatory power (Hobday et al., 2011). This is particularly apparent at Smoky Cape (31 °S). Here, the EAC speeds up and often encroaches onto the shelf, displacing shelf waters offshore, resulting in some of the lowest Chl. *a* on the shelf (Table 2). At Smoky Cape, water is upwelled onto the slope but doesn't reach the surface until further to the south (Roughan and Middleton, 2002; Oke and Middleton, 2001) where the shelf is productive, supporting significantly different larval fish communities (Syahailatua et al., 2011a; Mullaney et al., 2011) and faster growth rates of larval silver trevally and yellowtail scad (Syahailatua et al., 2011b) compared to sites

further offshore or periods of no upwelling.

South of the separation zone ($\sim$ 32°S), the coastline turns south-westward away from the EAC flow, forming Stockton Bight (32.25-33.25 °S), where reduced velocities and a wide shelf area (Fig. 1B) allows for retention and concentration of enriched waters moving south (Fig 4B). Stockton Bight is a biologically important area, with elevated nitrate (Suthers et al., 2011) and persistently high abundances of white sharks (Reid et al., 2011). Over the period of this study, Stockton Bight contained $\geq$20 % of the total shelf Chl. *a* on 27 % of occasions, highlighting its significance to the trophic ecology of the continental shelf. Additionally, the enriched shelf waters are often entrained into frontal cyclonic eddies which are generated by the EAC near Stockton Bight (Everett et al., 2011). These enriched eddies may act as incubators of zooplankton and larval fish (Mullaney and Suthers, 2013). Similar retention zones have been identified in other WBCs such as the Aghulus Current and Kuroshio Current. In the Aghulus Current, the Natal Bight is analogous to the Stockton Bight which also creates the necessary conditions for enhanced survivorship through lower velocities, some upwelling and enhanced phytoplankton levels (Hutchings et al., 2002). The Natal Bight is an important nursery ground for species such as the sparid *Chrysoblephus puniceus* (Hutchings et al., 2002) and like Stockton Bight, is protected from the higher velocities of the main current, allowing juveniles spawned in shelf waters to be retained and transported southwards at a much slower velocity. Similar conditions are also observed adjacent to the Kuroshio Current in the Enshu-nada Sea, one of the well-known spawning and nursery habitats off the central Pacific coast of Japan (Nakata et al., 2000). In the Enshu-nada Sea, a recirculation develops which initially transports sardine and anchovy eggs and larvae westward away from the main current, allowing for greater residence time on the shelf (Kasai

et al., 2002).

4.4 Limitations of estimating chlorophyll a from satellites

There are significant limitations to the use of satellite Chl. *a*, particularly with respect to absolute compared to relative values, the optical properties of the water, the differing absorbance of Chl. *a* due to phytoplankton species composition and cell-size and the estimation of subsurface phytoplankton biomass (Dierssen, 2010). Where possible, we have attempted to reduce the impact of these limitations on our results in order to progress our understanding of temporal and spatial patterns in Chl. *a*. In this study we compared relative values of remotely sensed Chl. *a* across a latitudinal gradient. By focussing on relative values and anomalies of Chl. *a* from a monthly climatology, and relating these values to the underlying drivers, we limit our reliance on the absolute magnitude of satellite-derived Chl. *a*. Additionally, optical properties of the water, such as the concentration of Colour Dissolved Organic Matter (CDOM) may interfere with remote measurements of Chl. *a*, however a review of global CDOM distributions show relatively low CDOM along the east Australian coast (Fig. 4 within Nelson and Siegel (2013)) which is consistent with our in-situ observations.

This examination of surface Chl. *a* focusses on significant upwelling events with a strong biological response. Our results show that a certain set of conditions (such as an upwelling-favourable wind and current) must be arranged in a favourable way for positive Chl. *a* anomalies to occur. Wind is an important component in this study, because it strongly influences the surface expression of Chl. *a*, and hence our ability to quantify it using these methods. The underlying physical mechanisms show why the observed patterns of surface Chl.

a exist. In addition, due to the southward flow of the EAC, upwelled water is often advected south, away from the initial location of upwelling. Both Cape Byron and Smoky Cape exhibit the highest proportion of upwelling-favourable conditions for the northern and central zones respectively, however the peaks in the long-term average Chl. *a* were seen approximately one degree further south.

Weaker upwelling events will also influence phytoplankton biomass at depth but were not quantified in this study. Measurements of subsurface Chl. *a* are necessary to fully describe the biological impact of upwelling events, however these measurements are less common and generally associated with infrequent research voyages within the region. The development of deep-chlorophyll maxima in response to oceanographic features, such as those observed by Gibbs (2000) and Tranter et al. (1986) off Sydney, are likely to play a role in the trophic ecology of this region and therefore need further investigation. In addition, the eventual fate of this Chl. *a* is little understood. We observe from satellite images (i.e. Fig. 2B) and process studies (Everett et al., 2011) that surface Chl. *a* signatures are often advected offshore as filaments or entrained into eddies. The majority of the offshore flux of phytoplankton across the 200 m isobath is shown to occur between 32 and 34 °S (See Fig. 17 from Baird et al. (2006)), but whether the advected phytoplankton is grazed down or sinks out is unclear.

5 Concluding remarks

The EAC region has the second fastest warming trend of all WBCs (Wu et al., 2012), with cascading changes to ecological communities such as zooplankton

populations and kelp beds already apparent (Johnson et al., 2011). As the EAC intensifies, patterns of upwelling and eddy generation are likely to change, but it is still unclear what the consequences of this are for ecosystem productivity. By developing an understanding of the current and historical patterns of phytoplankton biomass, we provide a process-based understanding of the drivers of phytoplankton dynamics along the EAC and can now speculate as to how greater southward penetration of the EAC will affect Chl. *a*.

Our analysis shows that in the southern zone, seasonal effects are more significant drivers of Chl. *a* than upwelling and EAC-derived eddies, suggesting that changes in the EAC may have less impact on lower trophic levels in this region. In the northern and central zones, it is likely that increased current-driven upwelling of nutrient-rich waters will result in greater surface Chl. *a*, but the higher EAC velocities in this region may lead to greater poleward advection, and hence dilution, of these enriched waters. Under this future scenario, zones of retention such as Stockton Bight, similar to the Enshu-nada Sea in the Kuroshio Current and the Natal Bight in the Aghulus Current, will likely have elevated biological significance.

6 Acknowledgements

JDE is partly supported by funding from the NSW Science Leveraging Fund. The authors thank Julie Wood, Amandine Schaeffer, Peter Oke and Matt Taylor for useful discussions about the data. BRAN output was sourced from the Integrated Marine Observing System (IMOS), an initiative of the Australian Government being conducted as part of the National Collaborative Research Infrastructure Strategy and the Super Science Initiative. We also acknowl-

edge the MODIS mission scientists and associated NASA personnel for the production of the data used in this research effort. We thank two anonymous reviewers who's comments greatly improved this manuscript. This manuscript number XXXX from the Sydney Institute of Marine Science.

References

Ajani, P. A., Lee, R., Pritchard, T., Krogh, M., 2001. Phytoplankton dynamics at a long-term coastal station off Sydney, Australia. Journal of Coastal Research ICS2000, 1–7.

Baird, M. E., Timko, P. G., Middleton, J. H., Mullaney, T. J., Cox, D. R., Suthers, I. M., 2008. Biological properties across the Tasman Front off south-east Australia. Deep Sea Research Part I: Oceanographic Research Papers 55 (11), 1438–1455.

Baird, M. E., Timko, P. G., Suthers, I. M., Middleton, J. H., 2006. Coupled physical-biological modelling study of the East Australian Current with idealised wind forcing: Part II. Biological dynamical analysis. Journal of Marine Systems 59 (3-4), 271–291.

Bakun, A., 1996. Patterns in the Ocean. Ocean processes and marine population dynamics. California Sea Grant College System/NOAA/Centro de Investigaciones Biologicas del Noroeste, La Paz, Mexico.

Bakun, A., Beyer, J., Pauly, D., Pope, J., Sharp, G., 1982. Ocean sciences in relation to living resources. Canadian Journal of Fisheries and Aquatic Sciences 39 (7), 1059–1070.

Banks, S. C., Piggott, L. M. P., Williamson, J. E., Bové, U., Holbrook, N. J., Beheregaray, L. B., 2007. Oceanic variability and coastal topography shape genetic structure in a long-dispersing sea urchin. Ecology 88 (12), 3055–64.

Bureau of Meteorology, 2012. Southern Oscillation Index.
URL http://www.bom.gFov.au/climate/current/soi2.shtml

Chelton, D. B., Schlax, M. G., Samelson, R. M., 2011. Global observations of nonlinear mesoscale eddies. Progress In Oceanography 91 (2), 167–216.

Cury, P., Jun. 2000. Small pelagics in upwelling systems: patterns of interaction and structural changes in wasp-waist ecosystems. ICES Journal of Marine Science 57 (3), 603–618.

Dierssen, H. M., 2010. Perspectives on empirical approaches for ocean color remote sensing of chlorophyll in a changing climate. Proceedings of the National Academy of Sciences of the United States of America 107 (40), 17073–8.

Everett, J. D., Baird, M. E., Oke, P. R., Suthers, I. M., 2012. An avenue of eddies: Quantifying the biophysical properties of mesoscale eddies in the Tasman Sea. Geophysical Research Letters 39, L16608.

Everett, J. D., Baird, M. E., Suthers, I. M., 2011. Three-dimensional structure of a swarm of the salp *Thalia democratica* within a cold-core eddy off southeast Australia. Journal of Geophysical Research 116 (C12), 1–14.

Fréon, P., Cury, P., 2005. Sustainable exploitation of small pelagic fish stocks challenged by environmental and ecosystem changes: a review. Bulletin of Marine Science 76 (2), 385–462.

Gibbs, M., 2000. Elevated chlorophyll a concentrations associated with a transient shelfbreak front in a western boundary current at Sydney, southeastern Australia. Marine and Freshwater Research 51 (8), 733–737.

Gibbs, M. T., Middleton, J. H., Marchesiello, P., 1998. Baroclinic response of Sydney shelf waters to local wind and deep ocean forcing. Journal of Physical Oceanography 28 (2), 178–190.

Godfrey, J., Cresswell, G., Golding, T., Pearce, A., Boyd, R., 1980. The sep-

aration of the East Australian Current. Journal of Physical Oceanography 10, 430–440.

Hallegraeff, G., Jeffrey, S., 1993. Annually recurrent diatom blooms in spring along the New South Wales coast of Australia. Marine and Freshwater Research 44 (2), 325–334.

Hassler, C. S., Djajadikarta, J., Doblin, M., Everett, J. D., Thompson, P. A., Mar. 2011. Characterisation of water masses and phytoplankton nutrient limitation in the East Australian Current separation zone during spring 2008. Deep Sea Research Part II: Topical Studies in Oceanography 58 (5), 664–677.

Hill, K. L., Rintoul, S. R., Ridgway, K. R., Oke, P. R., 2011. Decadal changes in the South Pacific western boundary current system revealed in observations and ocean state estimates. Journal of Geophysical Research 116 (C1), 1–12.

Hobday, A. J., Hartmann, K., 2006. Near real-time spatial management based on habitat predictions for a longline bycatch species. Fisheries Management and Ecology 13 (6), 365–380.

Hobday, A. J., Young, J. W., Moeseneder, C., Dambacher, J., Mar. 2011. Defining dynamic pelagic habitats in oceanic waters off eastern Australia. Deep Sea Research Part II: Topical Studies in Oceanography 58 (5), 734–745.

Hutchings, L., Beckley, L., Griffiths, M., Roberts, M., Sundby, S., van der Lingen, C., 2002. Spawning on the edge: spawning grounds and nursery areas around the southern African coastline. Marine and Freshwater Research 53, 307–318.

Johnson, C. R., Banks, S. C., Barrett, N. S., Cazassus, F., Dunstan, P. K., Edgar, G. J., Frusher, S. D., Gardner, C., Haddon, M., Helidoniotis, F., Hill, K. L., Holbrook, N. J., Hosie, G. W., Last, P. R., Ling, S. D., Melbourne-

Thomas, J., Miller, K., Pecl, G. T., Richardson, A. J., Ridgway, K. R., Rintoul, S. R., Ritz, D. A., Ross, D. J., Sanderson, J. C., Shepherd, S. A., Slotwinski, A., Swadling, K. M., Taw, N., 2011. Climate change cascades: Shifts in oceanography, species' ranges and subtidal marine community dynamics in eastern Tasmania. Journal of Experimental Marine Biology and Ecology 400 (1-2), 17–32.

Kasai, A., Kimura, S., Nakata, H., Okazaki, Y., 2002. Entrainment of coastal water into a frontal eddy of the Kuroshio and its biological significance. Journal of Marine Systems 37 (1-3), 185–198.

Kim, W., Yeh, S.-W., Kim, J.-H., Kug, J.-S., Kwon, M., 2011. The unique 2009-2010 El Niño event: A fast phase transition of warm pool El Niño to La Niña. Geophysical Research Letters 38 (15), 1–5.

Largier, J. L., Lawrence, C. A., Roughan, M., Kaplan, D. M., Dever, E. P., Dorman, C. E., Kudela, R. M., Bollens, S. M., Wilkerson, F. P., Dugdale, R. C., Botsford, L. W., Garfield, N., Kuebel Cervantes, B., Koračin, D., 2006. WEST: A northern California study of the role of wind-driven transport in the productivity of coastal plankton communities. Deep Sea Research Part II: Topical Studies in Oceanography 53 (25-26), 2833–2849.

Loder, J. W., Boicourt, W. C., Simpson, J. H., 1998. Western Ocean Boundary Shelves Coastal Segment. In: Robinson, A. R., Brink, K. H. (Eds.), The Sea, Volume 11. John Wiley Sons, Inc., pp. 3–27.

Logerwell, E. A., Smith, P. E., 2001. Mesoscale eddies and survival of late stage Pacific sardine (*Sardinops sagax*) larvae. Fisheries Oceanography 10 (1), 13–25.

Mouw, C. B., Yoder, J. A., 2005. Primary production calculations in the Mid-Atlantic Bight, including effects of phytoplankton community size structure. Limnology and Oceanography, 1232–1243.

623 Mullaney, T. J., Miskiewicz, A. G., Baird, M. E., Burns, P. T. P., Suthers,
624 I. M., 2011. Entrainment of larval fish assemblages from the inner shelf into
625 the East Australian Current and into the western Tasman Front. Fisheries
626 Oceanography 20 (5), 434–447.
627 Mullaney, T. J., Suthers, I. M., 2013. Entrainment and retention of the coastal
628 larval fish assemblage by a short-lived, submesoscale, frontal eddy of the
629 East Australian Current. Limnology and Oceanography.
630 Nakata, H., Kimura, S., Okazaki, Y., Kasai, A., 2000. Implications of meso-
631 scale eddies caused by frontal disturbances of the Kuroshio Current for
632 anchovy recruitment. ICES Journal of Marine Science 57 (1), 143–152.
633 Nelson, N. B., Siegel, D. A., 2013. The Global Distribution and Dynamics of
634 Chromophoric Dissolved Organic Matter. Annual Review of Marine Science
635 5 (1), 447–476.
636 Nilsson, C., Cresswell, G., 1981. The formation and evolution of East Aus-
637 tralian Current warm-core eddies. Progress in Oceanography 9 (3), 133–183.
638 Oke, P. R., Brassington, G. B., Griffin, D. A., Schiller, A., 2008. The Bluelink
639 ocean data assimilation system (BODAS). Ocean Modelling 21 (1-2), 46–70.
640 Oke, P. R., Griffin, D. A., Schiller, A., Matear, R. J., Fiedler, R., Mansbridge,
641 J., Lenton, A., Cahill, M., Chamberlain, M. A., Ridgway, K. R., 2012. Eval-
642 uation of a near-global eddy-resolving ocean model. Geoscientific Model
643 Development Discussions 5 (4), 4305–4354.
644 Oke, P. R., Middleton, J. H., 2000. Topographically induced upwelling off
645 eastern Australia. Journal of Physical Oceanography 30 (3), 512–531.
646 Oke, P. R., Middleton, J. H., 2001. Nutrient enrichment off Port Stephens: the
647 role of the East Australian Current. Continental Shelf Research 21 (6-7),
648 587–606.
649 Oke, P. R., Sakov, P., Cahill, M. L., Dunn, J. R., Fiedler, R., Griffin, D. A.,

650 Mansbridge, J. V., Ridgway, K. R., Schiller, A., 2013. Ocean Modelling.
651 Ocean Modelling 67 (C), 52–70.
652 Oke, P. R., Schiller, A., Griffin, D. A., Brassington, G. B., Oct. 2005. Ensem-
653 ble data assimilation for an eddy-resolving ocean model of the Australian
654 region. Quarterly Journal of the Royal Meteorological Society 131 (613),
655 3301–3311.
656 Olson, D. B., Jun. 2001. Biophysical dynamics of western transition zones: a
657 preliminary synthesis. Fisheries Oceanography 10 (2), 133–150.
658 Pauly, D., Christensen, V., 1995. Primary production required to sustain
659 global fisheries. Nature 374 (6519), 255–257.
660 Reid, D., Robbins, W., Peddemors, V., 2011. Decadal trends in shark catches
661 and effort from the New South Wales , Australia , Shark Meshing Program.
662 Marine and Freshwater Research 62, 676–693.
663 Revill, A. T., Young, J. W., Lansdell, M., 2009. Stable isotopic evidence for
664 trophic groupings and bio-regionalization of predators and their prey in
665 oceanic waters off eastern Australia. Marine Biology 156 (6), 1241–1253.
666 Ridgway, K. R., Godfrey, J., 1997. Seasonal cycle of the East Australian Cur-
667 rent. Journal of Geophysical Research 102 (C10), 22921–22.
668 Rossi, V., Schaeffer, A., Wood, J., Galibert, G., Sudre, J., Morris, B., Roughan,
669 M., Waite, A., submitted. Seasonality of sporadic physical processes driv-
670 ing temperature and nutrient variability in the coastal ocean: a multi-sensor
671 approach over the southeast Australian continental shelf. Journal of Geo-
672 physical Research - Oceans.
673 Roughan, M., Macdonald, H. S., Baird, M. E., Glasby, T. M., 2011. Modelling
674 coastal connectivity in a Western Boundary Current: Seasonal and inter-
675 annual variability. Deep Sea Research Part II: Topical Studies in Oceanog-
676 raphy 58 (5), 628–644.

677 Roughan, M., Middleton, J., 2004. On the East Australian Current: Variabil-
678 ity, encroachment, and upwelling. Journal of Geophysical Research 109 (C7).
679 Roughan, M., Middleton, J. H., 2002. A comparison of observed upwelling
680 mechanisms off the east coast of Australia. Continental Shelf Research
681 22 (17), 2551–2572.
682 Ryther, J. H., 1969. Photosynthesis and fish production in the sea. Science
683 166 (3901), 72–6.
684 Schaeffer, A., Roughan, M., Morris, B. D., 2013. Cross-shelf dynamics in a
685 Western Boundary Current regime: Implications for upwelling. Journal of
686 Physical Oceanography 43 (5), 1042–1059.
687 Schiller, A., Oke, P. R., Brassington, G. B., Entel, M., Fiedler, R., Grif-
688 fin, D. A., Mansbridge, J., 2008. Eddy-resolving ocean circulation in the
689 Asian-Australian region inferred from an ocean reanalysis effort. Progress
690 In Oceanography 76 (3), 334–365.
691 Seymour, J. R., Doblin, M. A., Jeffries, T. C., Brown, M. V., Newton, K.,
692 Ralph, P. J., Baird, M., Mitchell, J. G., 2012. Contrasting microbial as-
693 semblages in adjacent water-masses associated with the East Australian
694 Current. Environmental Microbiology Reports 4, 548555.
695 Suthers, I. M., Young, J. W., Baird, M. E., Roughan, M., Everett, J. D.,
696 Brassington, G. B., Byrne, M., Condie, S. A., Hartog, J. R., Hassler, C. S.,
697 2011. The strengthening East Australian Current, its eddies and biological
698 effects an introduction and overview. Deep Sea Research Part II: Topical
699 Studies in Oceanography 58 (5), 538–546.
700 Syahailatua, A., Roughan, M., Suthers, I. M., 2011a. Characteristic ichthy-
701 oplankton taxa in the separation zone of the East Australian Current: Lar-
702 val assemblages as tracers of coastal mixing. Deep Sea Research Part II:
703 Topical Studies in Oceanography 58 (5), 678–690.

Syahailatua, A., Taylor, M. D., Suthers, I. M., 2011b. Growth variability and stable isotope composition of two larval carangid fishes in the East Australian Current: The role of upwelling in the separation zone. Deep Sea Research Part II: Topical Studies in Oceanography 58 (5), 691–698.

Thompson, P. A., Baird, M. E., Ingleton, T., Doblin, M., 2009. Long-term changes in temperate Australian coastal waters: implications for phytoplankton. Marine Ecology Progress Series 394, 1–19.

Torrence, C., Compo, G. P., 1998. A practical guide to wavelet analysis. Bulletin of the American Meteorological Society 79 (1), 61–78.

Tranter, D., Carpenter, D., Leech, G., 1986. The coastal enrichment effect of the East Australian Current eddy field. Deep Sea Research Part A. Oceanographic Research Papers 33 (11-12), 1705–1728.

Uppala, S. M., Kllberg, P. W., Simmons, A. J., Andrae, U., Bechtold, V. D. C., Fiorino, M., Gibson, J. K., Haseler, J., Hernandez, A., Kelly, G. A., Li, X., Onogi, K., Saarinen, S., Sokka, N., Allan, R. P., Andersson, E., Arpe, K., Balmaseda, M. A., Beljaars, A. C. M., Berg, L. V. D., Bidlot, J., Bormann, N., Caires, S., Chevallier, F., Dethof, A., Dragosavac, M., Fisher, M., Fuentes, M., Hagemann, S., Hlm, E., Hoskins, B. J., Isaksen, L., Janssen, P. A. E. M., Jenne, R., Mcnally, A. P., Mahfouf, J.-F., Morcrette, J.-J., Rayner, N. A., Saunders, R. W., Simon, P., Sterl, A., Trenberth, K. E., Untch, A., Vasiljevic, D., Viterbo, P., Woollen, J., 2005. The era-40 reanalysis. Quarterly Journal of the Royal Meteorological Society 131 (612), 2961–3012.

Ware, D. M., Thomson, R. E., 2005. Bottom-up ecosystem trophic dynamics determine fish production in the northeast Pacific. Science 308 (5726), 1280–1284.

Winder, M., Cloern, J., 2010. The annual cycles of phytoplankton biomass.

731 Philosophical Transactions of the Royal Society B: Biological Sciences
732 365 (1555), 3215–3226.
733 Wood, J. E., Roughan, M., Tate, P. M., 2012. Finding a proxy for wind stress
734 over the coastal ocean. Marine and Freshwater Research 63 (6), 528.
735 Wu, L., Cai, W., Zhang, L., Nakamura, H., Timmermann, A., Joyce, T.,
736 McPhaden, M. J., Alexander, M., Qiu, B., Visbeck, M., Chang, P., Giese, B.,
737 Jan. 2012. Enhanced warming over the global subtropical western boundary
738 currents. Nature Climate Change 2 (1), 1–6.

Table 1
Physical properties of each latitudinal band showing the closest population centre, shelf area (A_{Sh}) and percent of total shelf area ($A_{\%}$), mean surface velocity ($\bar{v}_{surf}$), and percentage of the time there is an upwelling or downwelling-favourable bottom stress (τ_b^{up} (τ_b^{do})) and wind stress (τ_w^{up} (τ_w^{do})) at the shelf edge. The average for each column is presented in the bottom row.

Latitude	Geographic Location	A_{Sh} ($A_{\%}$) km^2 (%)	$\bar{v}_{surf}$ m s^{-1}	τ_w^{up} (τ_w^{do}) % (%)	τ_b^{up} (τ_b^{do}) % (%)
-28	Gold Coast	2271 (4)	0.62	9 (32)	41 (0)
-28.5	Cape Byron	1563 (3)	0.72	14 (33)	60 (1)
-29	Evans Head	1893 (6)	0.74	14 (31)	32 (3)
-29.5	Yamba	2332 (6)	0.50	15 (28)	47 (2)
-30	Coffs Harbour	1838 (4)	0.36	14 (25)	15 (4)
-30.5	Urunga	1643 (4)	0.43	17 (27)	30 (6)
-31	Smoky Cape	1213 (2)	0.49	17 (27)	43 (11)
-31.5	Laurieton	1480 (4)	0.60	15 (24)	29 (7)
-32	Diamond Head	2435 (8)	0.52	20 (26)	38 (5)
-32.5	Seal Rocks	2783 (7)	0.43	19 (26)	35 (8)
-33	Newcastle	4044 (10)	0.31	20 (26)	8 (7)
-33.5	Pittwater	3074 (6)	0.27	15 (26)	12 (14)
-34	Sydney	2061 (4)	0.29	11 (22)	13 (11)
-34.5	Wollongong	1749 (4)	0.32	9 (20)	25 (10)
-35	Jervis Bay	1791 (4)	0.38	11 (22)	46 (6)
-35.5	Ulladulla	1832 (5)	0.29	12 (19)	13 (5)
-36	Narooma	1474 (4)	0.30	12 (18)	16 (12)
-36.5	Bermagui	1223 (3)	0.39	13 (21)	29 (22)
-37	Eden	1814 (6)	0.36	15 (26)	23 (24)
-37.5	Gabo Island	1904 (7)	0.38	19 (36)	20 (44)
	Average:	2021	0.43	14 (28)	41 (19)

Table 2
Geometric mean Chl. *a* (mg m^{-3}) and standard deviation (SD) for each latitudinal band in the study domain. The mean percentage of total shelf Chl. *a* and spring increase (SI) for each latitude is also shown. The average for the entire shelf is presented in the bottom row.

Latitude	Chlorophyll *a* Av. (mg m^{-3})	Chlorophyll *a* S.D. –	Proportion Shelf Chl. *a* (%)	Spring Increase (%)
-28.00	0.26	2.19	3.93	28.92
-28.50	0.26	2.30	2.55	41.77
-29.00	0.38	2.81	5.76	64.77
-29.50	0.38	2.61	6.49	47.30
-30.00	0.35	2.32	3.96	41.13
-30.50	0.36	2.36	3.81	27.29
-31.00	0.30	2.25	2.02	42.78
-31.50	0.37	2.54	3.79	28.66
-32.00	0.44	2.70	8.47	79.09
-32.50	0.40	2.39	7.06	106.52
-33.00	0.38	2.23	9.94	68.41
-33.50	0.33	1.99	5.97	52.34
-34.00	0.31	1.92	3.38	51.69
-34.50	0.33	2.15	3.62	70.02
-35.00	0.38	2.37	3.94	101.77
-35.50	0.42	2.49	4.97	144.17
-36.00	0.41	2.46	4.06	150.01
-36.50	0.45	2.43	3.45	151.93
-37.00	0.46	2.37	5.68	145.40
-37.50	0.55	2.12	7.16	75.94
Average:	0.3828	2.4534	–	75.99

Table 3
The percentage of occasions that positive Chl. *a* anomalies result from a combination of wind (τ_W) and bottom stress (τ_B) induced upwelling/downwelling conditions at 32–33.5 °S. These latitudinal bands correspond to the region with a large response to upwelling events in Fig. 5. The bracket numbers indicate the number of occurrences of each combination.

	Upwelling τ_W	Neutral τ_W	Downwelling τ_W
Upwelling τ_B	65% (51)	37% (122)	38% (52)
Neutral τ_B	47% (117)	34% (371)	35% (173)
Downwelling τ_B	58% (12)	44% (43)	24% (29)

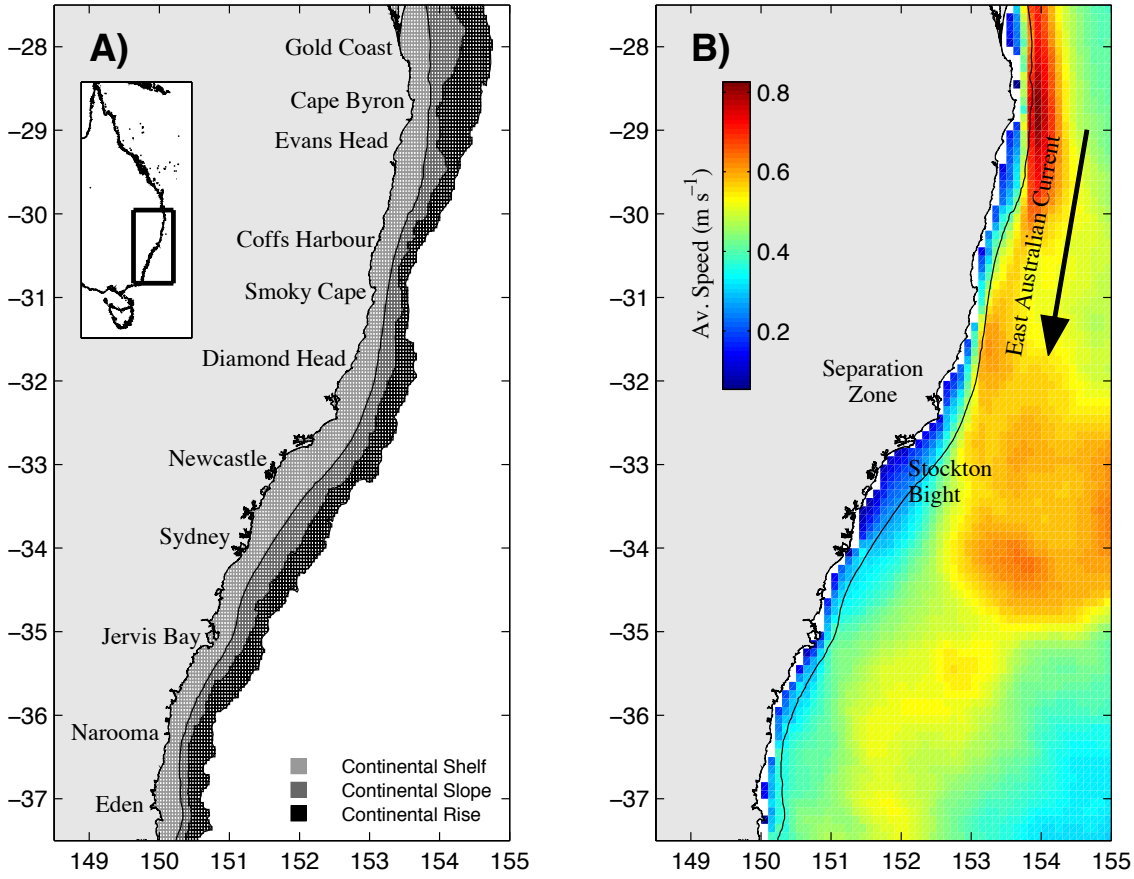

Fig. 1. Location map of southeast Australia showing A) the location of the continental shelf (0-200 m), continental slope (200-2000 m) and continental rise (2000-4000 m) as used for this analysis and B) The average surface velocities from the eddy-resolving global ocean model - Bluelink Reanalysis (BRAN; 2003-2008). The locations in A) link with Table 1. Regions of interest are marked on B) including the EAC separation zone, the core of the East Australian Current and the location of Stockton Bight. The thin black line indicates the edge of the continental shelf (200 m).

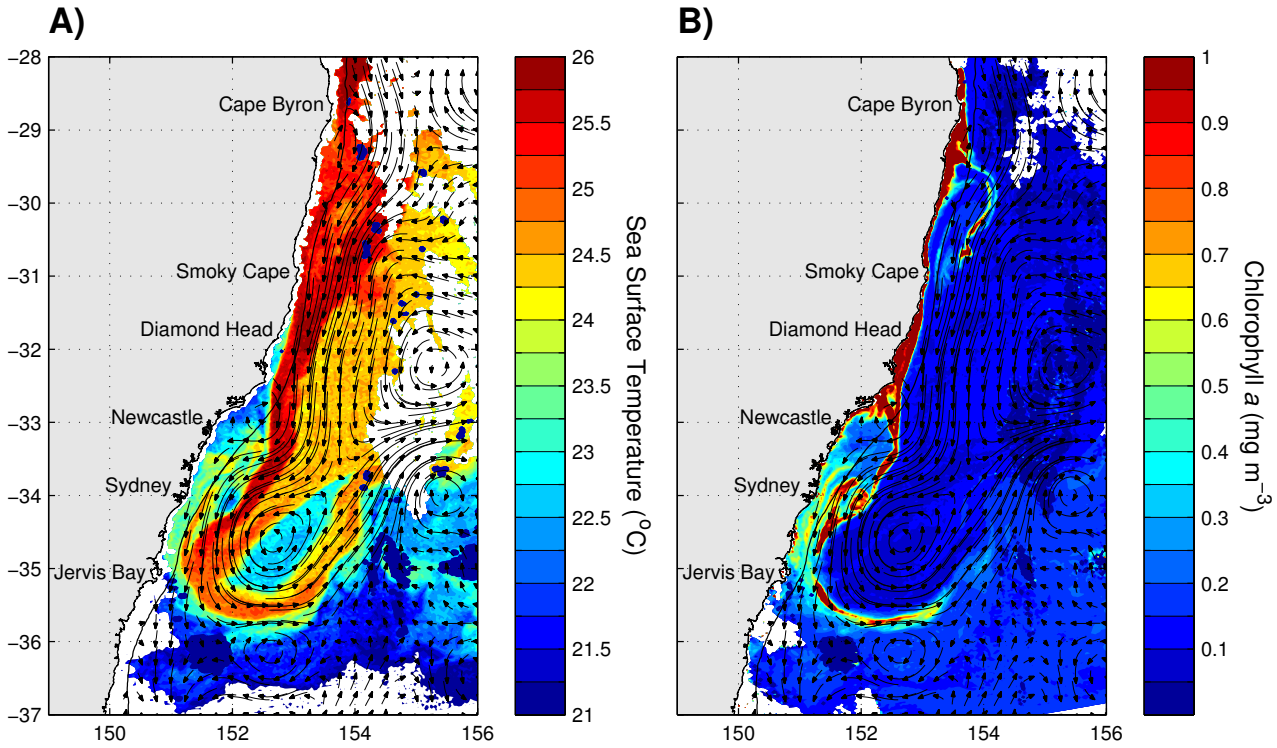

Fig. 2. Satellite image of the study region showing A) Sea Surface Temperature and B) Chlorophyll *a* from MODIS-Aqua Ocean Colour on 15th April 2009. The image is representative of many of the persistent oceanographic features of the region, including the EAC separation zone (32-33 °S), the EAC retroflection (34-35°S) and upwelling zones south of Cape Byron and Smoky Cape (visible as high chlorophyll *a* in B)). The arrows represent the geostrophic velocity derived from AVISO altimetry.

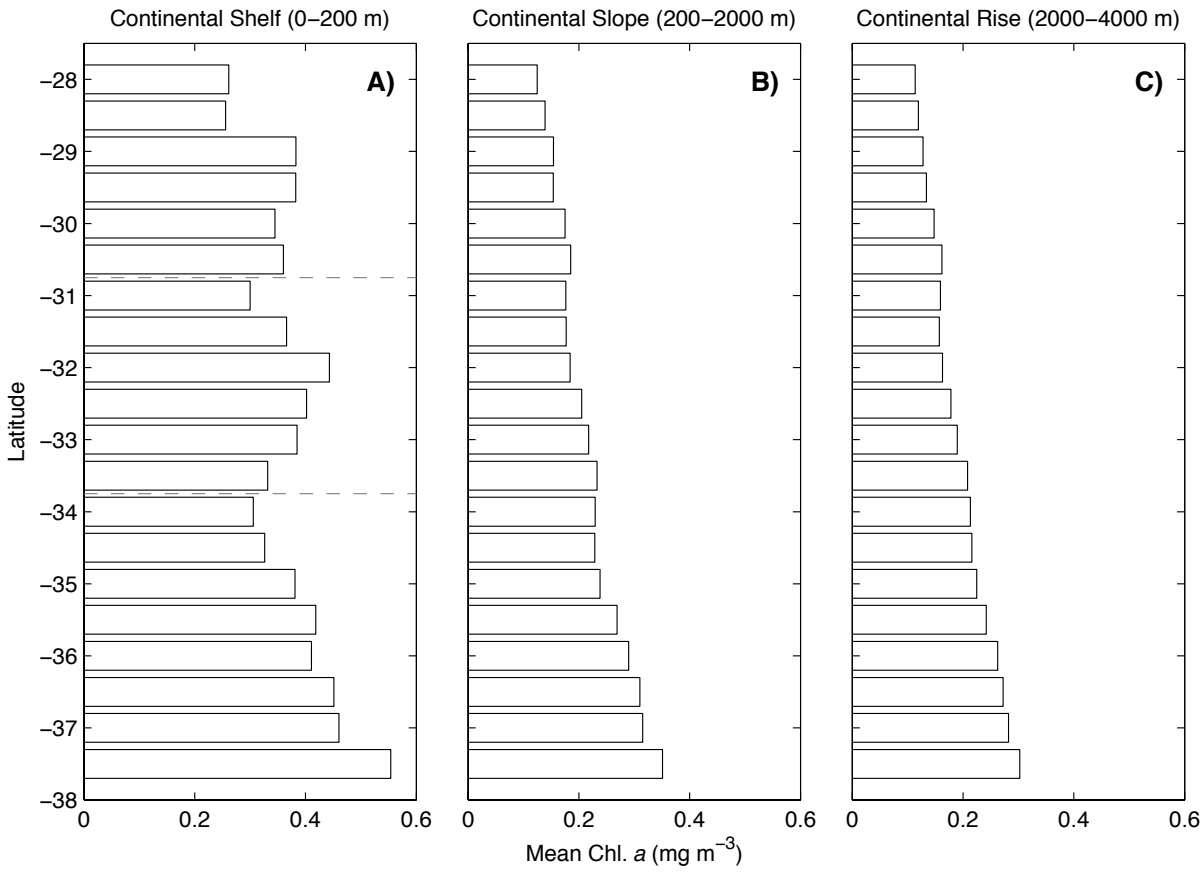

Fig. 3. Long-term mean Chl. *a* calculated for the study period (2003-2010) for 0.5 degree latitudinal bands. Data is partitioned based upon bathymetry, for the A) continental shelf (0-200 m), B) continental slope (200-2000 m) and C) continental rise (2000-4000 m). The dashed grey line indicates the boundaries of the northern, central and southern zones as defined in the results.

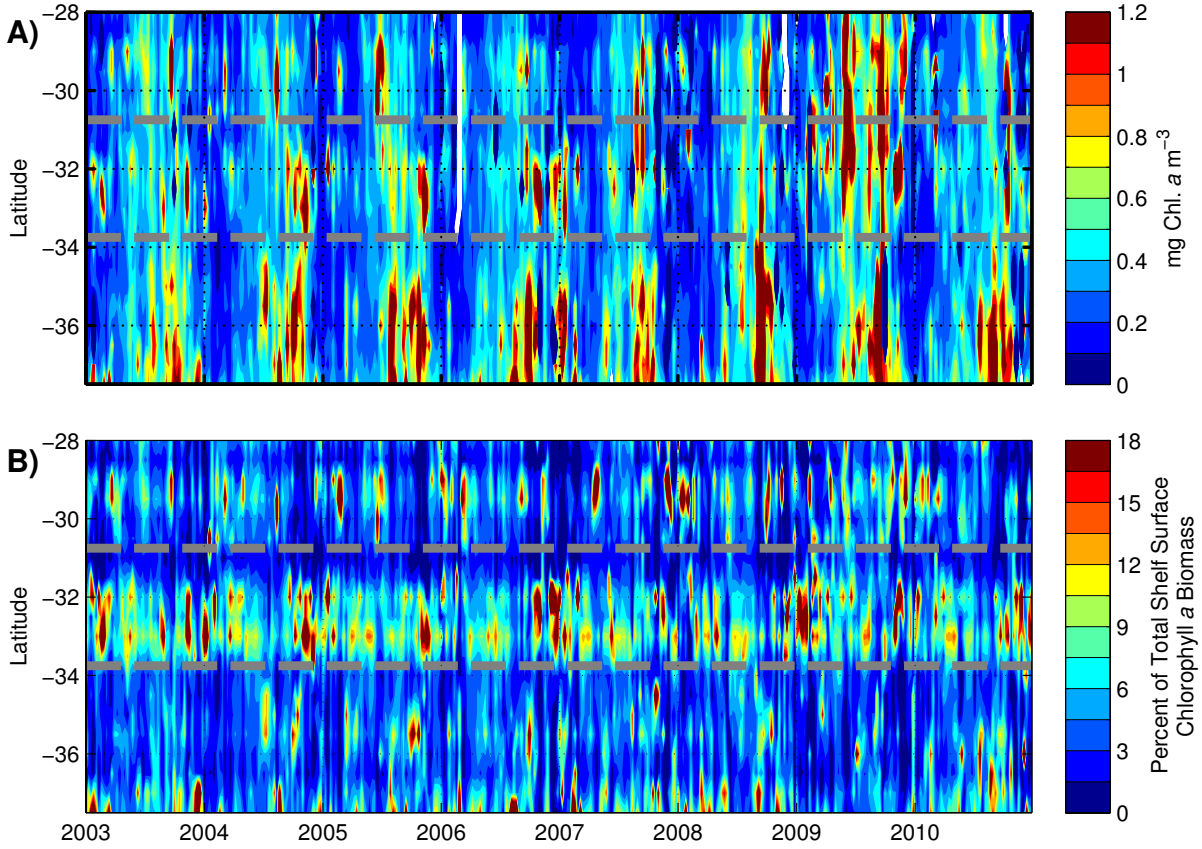

Fig. 4. A) Mean Chl. *a* (8-day composite) for all latitudinal bands within the study domain (2003-2010) and B) Percentage of total shelf Chl. *a*, for each latitudinal band (2003-2010). Total shelf Chl. *a* is the sum of all pixels on the shelf within each latitudinal band. The data is presented as a percentage of total shelf Chl. *a* for each time-step. The white sections represent missing data and the dashed grey line indicates the boundaries of the northern, central and southern zones as defined in the results.

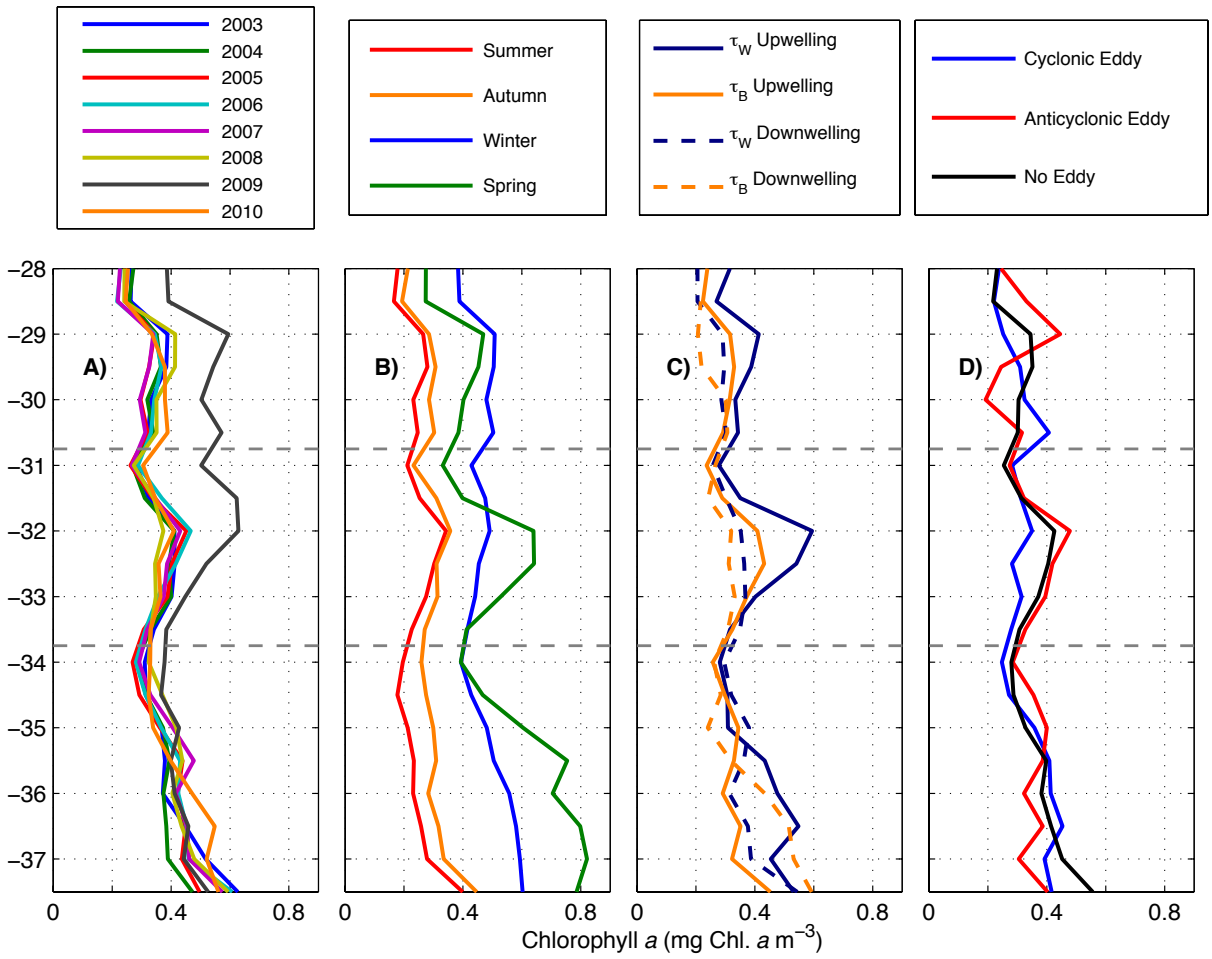

Fig. 5. Mean Chl. a for each latitudinal band presented as a temporal-average for A) Year, B) Season, C) Upwelling and downwelling-favourable wind (τ_W) and bottom (τ_B) stress and D) Eddy encroachment (Eddy edge <50 km to the continental shelf). The dashed grey line indicates the boundaries of the northern, central and southern zones as defined in the results. Due to the availability of output from BRAN, bottom-stress and wind-stress are calculated for 2003-2008. The Chl. a and eddy characteristics are calculated for the period 2003-2010, in order to use all the available data.

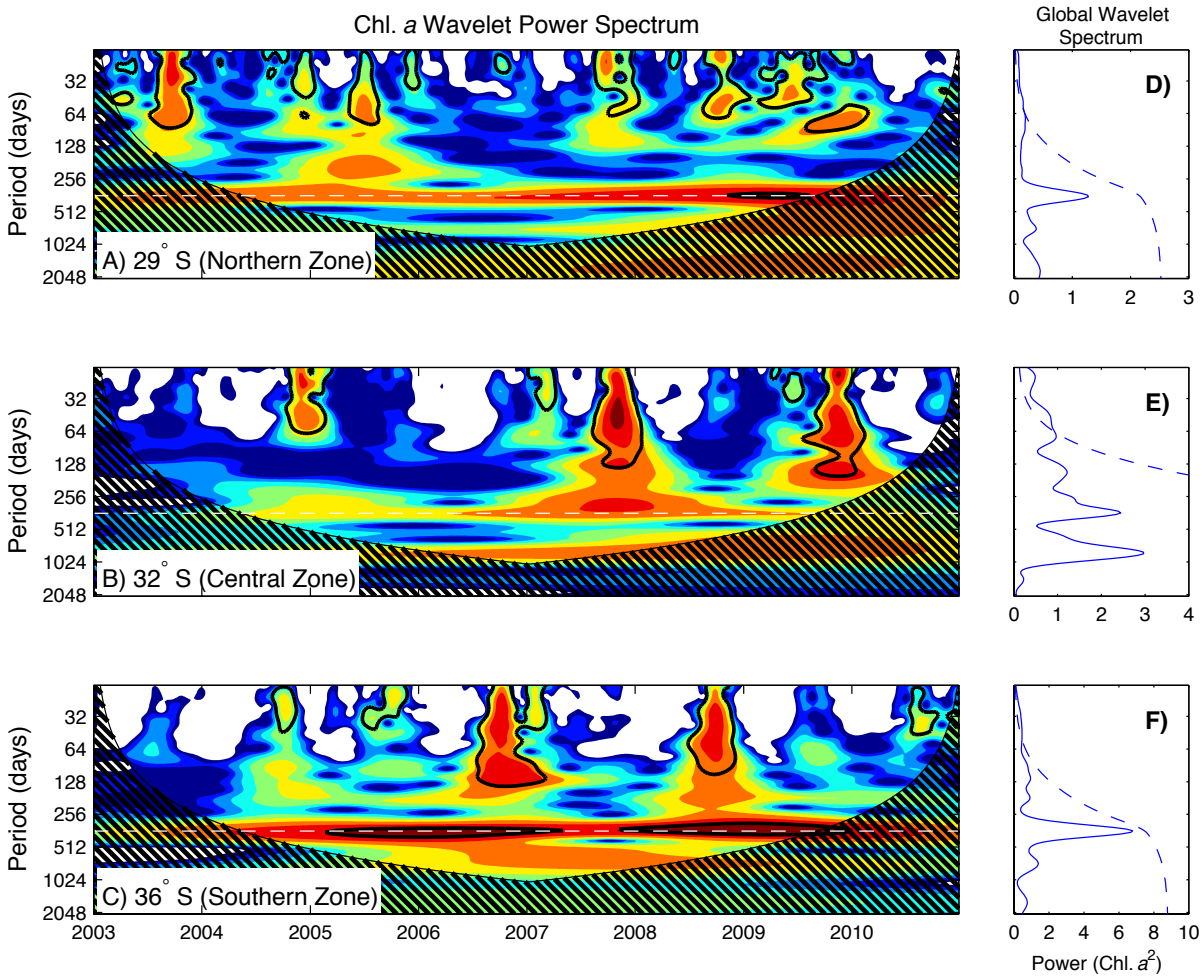

Fig. 6. The wavelet power spectrum (A-C) and Global Power Spectrum (D-F) showing the significant modes of variability in the 8-day Chl. *a* dataset for three latitudinal bands. The wavelet power spectrum (A-C) uses a Morlet wavelet function to estimate the frequency of variability. The x-axis is the wavelet location in time and the y-axis is the wavelet period in days. The black contours are the 5% significance regions, using a red-noise background spectrum. The black-hatched region indicates the cone of influence where edge effects are important and the dashed white line indicates a period of 365 days. Colours indicate differing degrees of variance (dark red indicates high intensity; dark blue indicates low intensity). The Global Power Spectrum (D-F) indicates the time-averaged intensity at each period. The period is considered significant where the Global Power Spectrum crosses the dashed line indicating the 95% confidence level (Torrence and Compo, 1998).

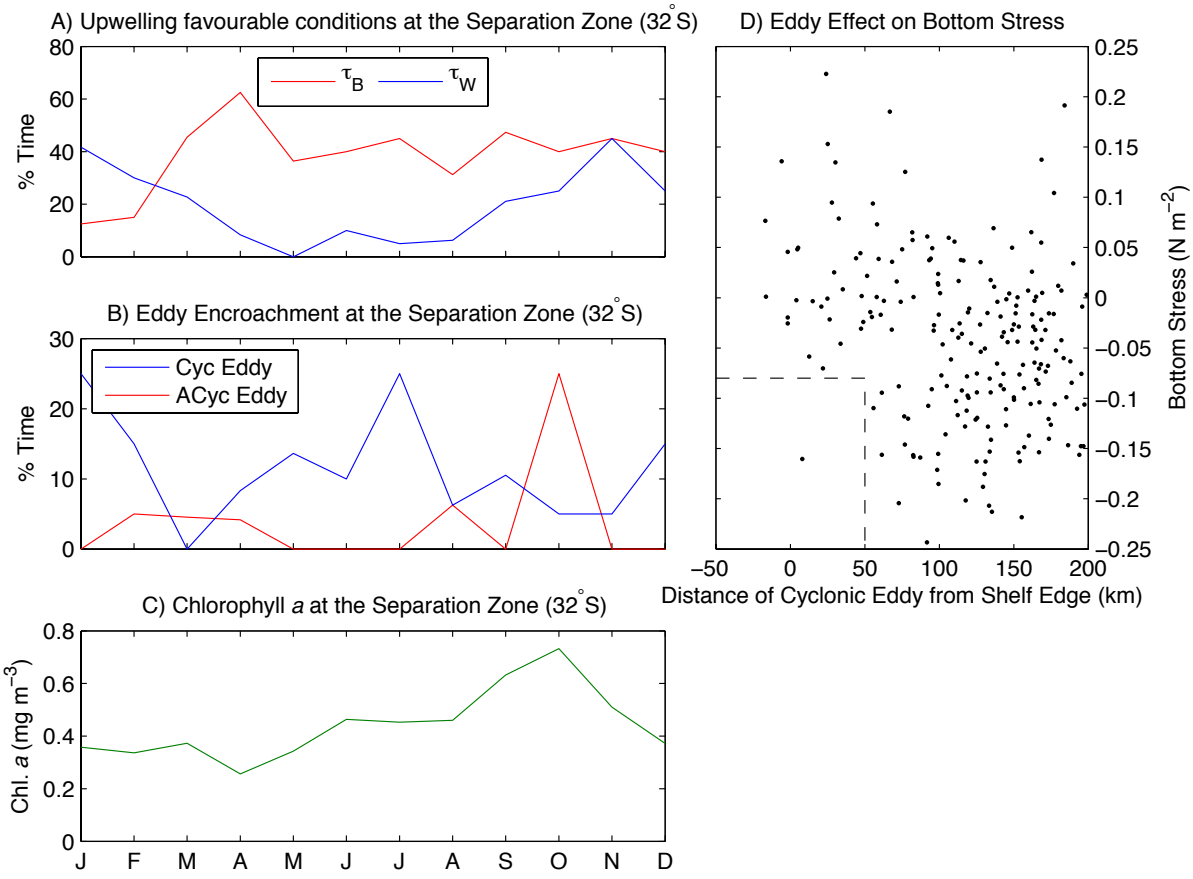

Fig. 7. Upwelling/Downwelling, Eddy and Chl. *a* characteristics at the separation zone (32 °S). Percentage of the time by month that A) Upwelling-favourable bottom- and wind-stress occurred and B) Cyclonic (Cyc) and Anticyclonic (ACyc) eddies came within 50 km of the shelf C) Average Chl. *a* is shown as a monthly mean and D) The cyclonic eddy-distance from the shelf-edge (as calculated from Chelton et al. (2011)) and BRAN bottom-stress from the shelf edge is presented. The region enclosed by the dashed line indicates where cyclonic eddies come within 50 km of the coast and an upwelling-favourable bottom-stress occurs. Distances in D) are calculated from the eddy edge to the shelf edge. Negative distances indicate the edge of the eddy has encroached onto the shelf. Due to the availability of BRAN output, bottom-stress and wind-stress are only calculated for 2003-2008. The Chl. *a* and eddy characteristics are calculated for the period 2003-2010, in order to use all the available data.

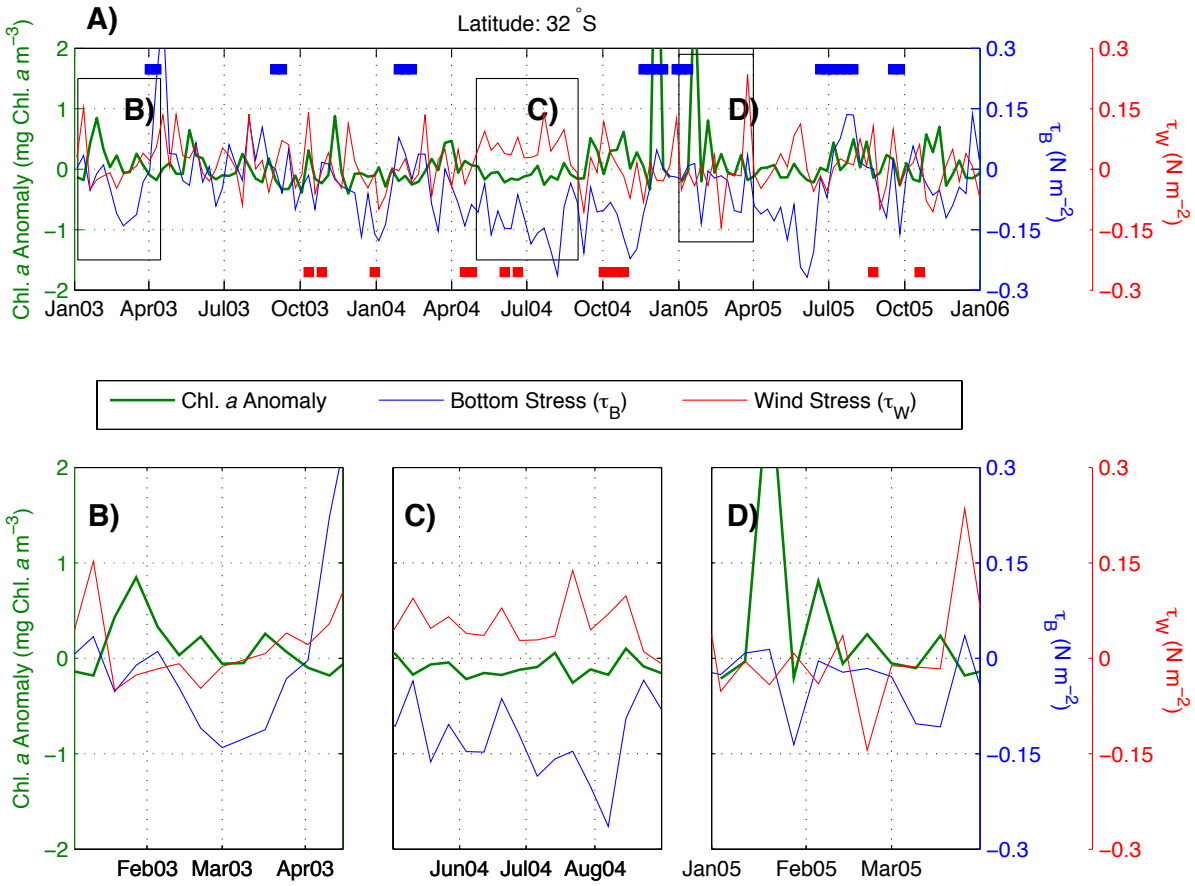

Fig. 8. A) Chl *a* anomaly relative to the monthly climatology (green-left axis), bottom stress (blue-right axis) and wind stress (red-right axis) are shown for the period Jan 2003 to Jan 2006. A negative bottom- and wind-stress corresponds to upwelling–favourable, and a positive bottom- and wind-stress is downwelling-favourable. The blue and red squares represent cyclonic and anticyclonic eddies respectively which encroach within 50 km of the shelf edge and are likely to have an impact on bottom-stress (Fig 7). Three time-periods (B-D) highlighted with blue boxes, and the corresponding area expanded at the bottom of the figure (Subplot B-D).

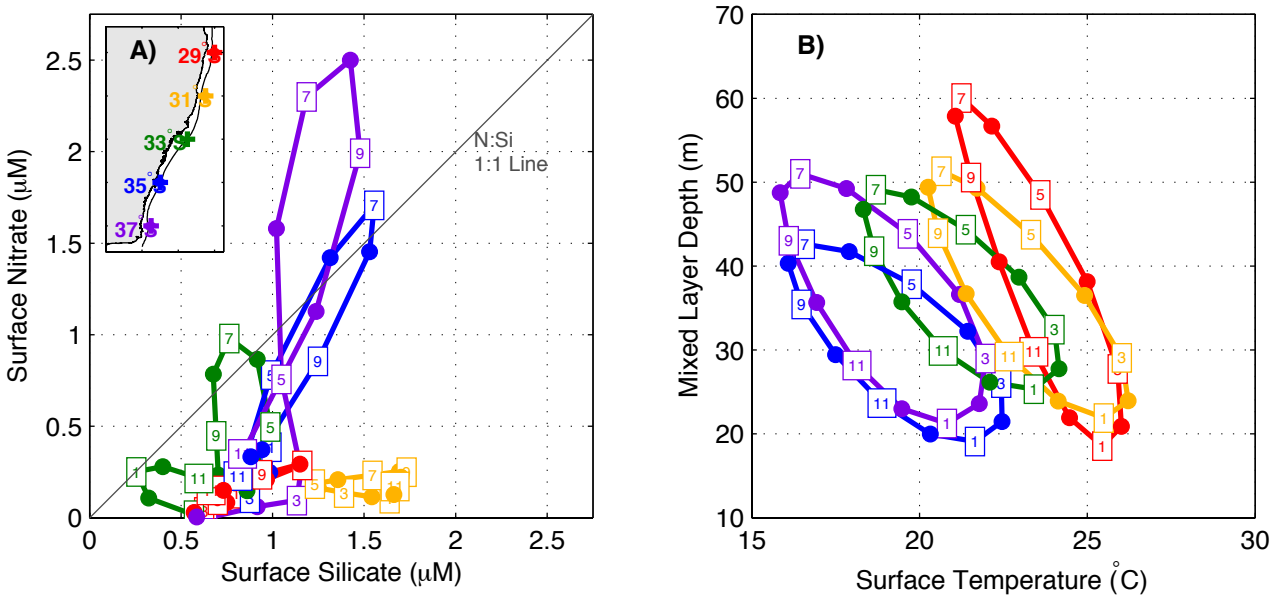

Fig. 9. Climatological properties of the southeast Australian continental shelf from the CSIRO Atlas of Regional Seas (CARS) version 2009 for A) Nitrate and Silicate and B) Mixed Layer Depth and Temperature. The plotted points are closest to the 200 m isobath at 29 °S, 31 °S, 33 °S, 35 °S and 37 °S. Month labels are centred on the 15th of each month. The insert shows the location of the CARS sites along the southeast Australian seaboard with the 200 m isobath drawn as a thin line.